


Article

Direct Thrust Force Control of Primary Permanent Magnet Linear Motor Based on Improved Extended State Observer and Model-Free Adaptive Predictive Control

Xiuping Wang¹, Shunyu Yao^{1,*}, Chunyu Qu¹, Yiming Wang², Zhangwei Xu³, Wenbin Huang³ and Hai Wang^{3,*} 

¹ School of Electric Power, Shenyang Institute of Engineering, Shenyang 110136, China

² Fuxin Power Supply Company, State Grid Liaoning Electric Power Company Limited, Fuxin 123000, China

³ Discipline of Engineering and Energy, Murdoch University, Perth, WA 6150, Australia

* Correspondence: 15712327235@163.com (S.Y.); hai.wang@murdoch.edu.au (H.W.)

Abstract: A model-free adaptive predictive control algorithm based on an improved extended state observer (IESO) is proposed to solve the problem that the primary permanent magnet linear motor is susceptible to time-varying parameters and unknown disturbances. Firstly, a model-free adaptive control algorithm based on compact format is designed to achieve high control precision of the system and reduce thrust fluctuation, only through the input/output data of the system. Because the traditional model-free adaptive control is too sensitive to the internal parameters of the controller, a combination of model-free adaptive control and predictive control is further developed. By predicting the data for a future time in advance, the sensitivity to the internal parameters of the controller is reduced and the control performance is further improved. Since the load change and other nonlinear disturbances in practical applications have a great impact on the control effect of the system, an improved extended state observer is further used to compensate for the impact of nonlinear disturbances on the control system. In addition, the stability of the closed-loop system is analyzed. Comparable simulation results clearly demonstrate the good tracking performance and strong robustness of the proposed control.

Keywords: primary permanent magnet linear motor (PPMLM); model-free adaptive control; predictive control; improved extended state observer (IESO)



Citation: Wang, X.; Yao, S.; Qu, C.; Wang, Y.; Xu, Z.; Huang, W.; Wang, H. Direct Thrust Force Control of Primary Permanent Magnet Linear Motor Based on Improved Extended State Observer and Model-Free Adaptive Predictive Control. *Actuators* **2022**, *11*, 270. <https://doi.org/10.3390/act11100270>

Academic Editor: Gary M. Bone

Received: 4 August 2022

Accepted: 19 September 2022

Published: 22 September 2022

Publisher's Note: MDPI stays neutral with regard to jurisdictional claims in published maps and institutional affiliations.



Copyright: © 2022 by the authors. Licensee MDPI, Basel, Switzerland. This article is an open access article distributed under the terms and conditions of the Creative Commons Attribution (CC BY) license (<https://creativecommons.org/licenses/by/4.0/>).

1. Introduction

In the past few years, in the field of modern urban rail transit, linear motors have become an indispensable traction method [1]. However, under the requirements of high performance and low cost, traditional linear motors cannot meet the needs of complex routes and low cost in urban rail transit and long journey requirements. Therefore, a primary permanent magnetic linear motor (PPMLM), as a new type of special motor, has been widely used in the field of rail transit. PPMLMs have the advantages of high power density, large thrust, high dynamic characteristics and acceleration of traditional linear motors. Because of their special structure, it reduces the cost of use when laying the track [2,3]. Direct thrust force control (DTFC), as the preferred control strategy for linear motor control systems in the field of rail transit, has the advantages of simple internal structure and fast response. However, owing to the internal structure of DTFC and the speed loop using a proportional–integral (PI) controller, its thrust fluctuation and steady-state error are relatively large. As such, it is necessary to design a controller with higher tracking accuracy to enable DTFC to have better tracking performance and smaller thrust fluctuation. In addition to overcoming the influence of the DTFC system, the currently designed controller also needs to consider that the special structure of PPMLM will make the control system vulnerable to uncertain nonlinearities such as internal parameter changes,

cogging effects, end effects, and saturation effects. Note that the influence of these factors leads to an increase in the difficulty of control [4–6].

Many scholars have put forward many solutions these problems, such as the relatively mature adaptive backlash control, sliding-mode variable structure control, and model predictive control. Ref. [7] proposed a control algorithm based on the combination of adaptive inverse control and radial-basis function (RBF) disturbance compensation technology, which improves the robustness and antidisturbance of the control system. Owing to the superior features of sliding-mode control in terms of high tracking accuracy and strong robustness [8–11], in Ref. [12], a nonlinear sliding-mode surface was designed to improve the response speed of the system, and the introduction of adaptive control gain not only weakened the chattering problem of the sliding-mode control itself, but also increased the tracking accuracy of the system. Ref. [13] proposed a complementary sliding-mode control to suppress the uncertain factors of linear motors, which effectively reduced the tracking error. Ref. [14] proposed a control method based on the combination of time-delay control and integral sliding mode, which not only decreases the influence of uncertainty on the control system but also improves the tracking performance of the system. Refs. [15–17] designed model predictive current control to replace the traditional current controller, which expanded the selection range of the voltage vector, and improved the current control accuracy and the control effect of the system. In order to further manage the issues of the negative effects of time-varying parameters and external disturbances on control systems, Ref. [18] proposed a fast, nonsingular terminal sliding-mode control method based on an extreme learning machine, which reduces the dependence on the mathematical model of the linear motor and thus reduces the influence of disturbance on control system. A compensation method based on an extended Kalman filter was proposed in [19] to estimate the initial position and mass change in the linear motor and adjust the motor model parameters in real time. Ref. [20] proposed to establish a mathematical model of a linear motor with uncertainty, and designed a periodic disturbance learning observer as the disturbance compensation for the control system to decrease the impact of external disturbances on the linear motor control system and improve the anti-interference of the system. In Ref. [21], an iterative proportional integral observer was proposed to estimate unknown disturbances and states of Markov jump systems, and a fuzzy fault-tolerant tracking control algorithm was designed according to the reconstructed fault states. In Ref. [22], an event-triggered control with an adaptive disturbance observer was designed for Markov jump systems to estimate multiple disturbances in the system, and then a composite state feedback controller was proposed according to the adaptability of the controller and compensator. Ref. [23] proposed a control method based on the combination of extended state observer and model predictive control. The extended state observer was used to estimate the disturbance that an underwater vehicle may encounter, and compensate for the disturbance effect caused by dynamic coupling inside and outside the system.

Considering the fact that a mathematical model is required for the control design described above, the control performance is somewhat affected if the modeling accuracy cannot be ensured. With the development of control theory, many scholars have proposed data-driven control methods for those systems that cannot be or are difficult to model accurately. The data-driven control method only uses the input/output (I/O) data of the system to design the controller, which can well avoid the control problems caused by the mathematical model. Ref. [24] proposed a deadbeat PI controller, which improves the decoupling capability of the motor control system, but the parameters need to be readjusted for the system in different situations. Ref. [25] designed a controller based on an adaptive wavelet-neural network. Although the self-learning capacity of the neural network has a good inhibitory effect on uncertainty, the neural network requires a large amount of data for training, leading to a relatively long training time. On this basis, Ref. [26] proposed to train the mathematical model of a switched reluctance motor using an RBF neural network and drive control. Because the motor mathematical model considers the internal coupling relationship of the motor, the control effect is better, but the amount of calculation required

for training the neural network is very large. Model-free adaptive control (MFAC) is a nonlinear control pattern with strong robustness. It uses the I/O data of the control object to evaluate a pseudo partial derivative (PPD) in real time, and then approximates expected values of the system [27,28]. Refs. [29,30] proposed MFAC methods that were applied to permanent magnet linear motors to verify their effectiveness. Further, Ref. [31] introduced iterative learning control into MFAC, which has a good suppression effect on the problem of strong coupling in the actual operation of two-dimensional linear motors. Ref. [32] applied the MFAC based on the partial format to the DTFC system of the PPMLM, which solved the problem of large thrust fluctuation in the DTFC system, and increased the universality compared with the MFAC of the compact format. Ref. [33] proposed to apply model-free adaptive predictive control to the motor control system, which improves the tracking accuracy of the system and increases noise interference, such that the feasibility of the proposed method is well verified under noise conditions. Ref. [34] applied model-free adaptive current control to the drive system of a wound-rotor synchronous machine, which has better control performance than a PI controller. Ref. [35] combined a multi-input and multi-output model-free adaptive control with virtual reference feedback control technology in the dual rotor control system, and verified the effectiveness of the combined control method.

Inspired by the aforementioned studies, this paper uses compact-form dynamic linearization model-free adaptive predictive control (CFDL–MFAPC) based on a direct thrust control system to optimize the speed loop of the PPMLM system. It is shown that the techniques of MFAPC and extended state observer are combined to further improve the control performance of the direct thrust control for PPMLM. Not only is the predictive control combined on the basis of MFAC, which makes it insensitive to parameter changes in the controller itself, but the speed-tracking accuracy is also further improved and the thrust pulsation reduced. Since the developed MFAPC does not require the mathematical model of PPMLM, it has a certain inhibitory effect on the changes in internal parameters of the system and external load disturbances.

For further eliminating the effects of fluctuations on the control performance, this work adopts an MFAPC method based on the improved extended state observer [36] (IESO) to increase the antidisturbance capability of the system and to further ensure excellent speed-control performance. Comparable simulation results are provided to thoroughly validate the good performance of the proposed control approach for the PPMLM system.

The remaining parts of this paper are organized as follows. Section 2 presents the system model of the PPMLM involving a DTFC system. In Section 3, few model-free adaptive control designs are described in detail, where the closed-loop stability proof is also given. Section 4 presents the simulation results to verify the effectiveness of the proposed controller. Section VI concludes this article.

2. PPMLM DTFC System

First, in the following paragraphs, the PPMLM direct thrust control system is established as the basis for optimizing the speed loop of the DTFC system. Figure 1 shows the block diagram of the DTFC system of PPMLM.

In Figure 1, v^* is reference speed; Δv is speed error; fe^* is control input; fe is the calculated motor thrust; Δfe is the thrust error; ψ_s^* is the given primary flux linkage; ψ_s is the calculated primary flux linkage; $\Delta \psi_s$ is the primary flux linkage error; $Sign_F$ is the thrust change signal; $Sign_Ψ$ is the magnetic link amplitude change signal; Sector is the magnetic link position signal; u_a, u_b, u_c is the primary three-phase terminal voltage; i_a, i_b, i_c is the primary three-phase winding current; and U_{dc} is the DC power supply.

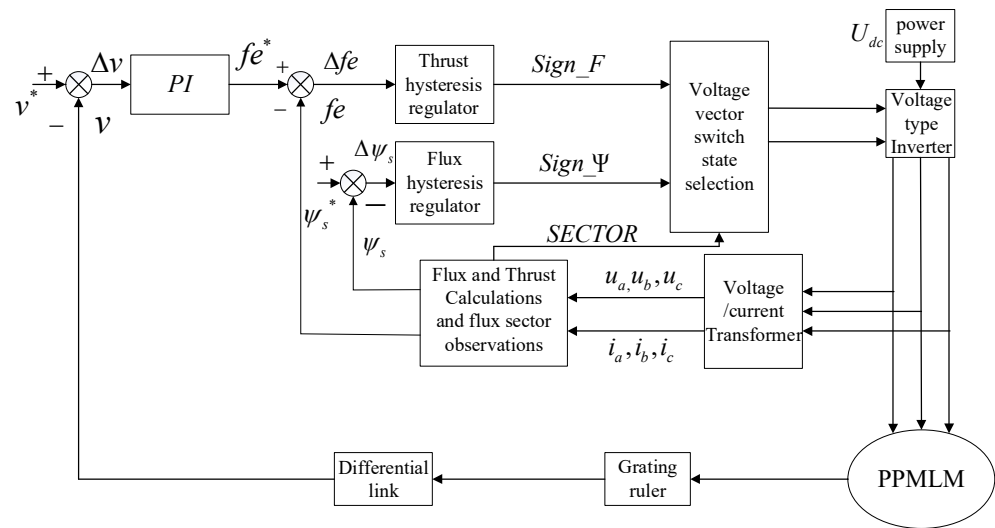


Figure 1. Block diagram of the direct thrust force control system for PPMLM.

The mathematical model of PPMLM follows:

$$\left. \begin{aligned} u_d &= R_s i_d + L_d \frac{di_d}{dt} - \frac{\pi v}{\tau} L_q i_q \\ u_q &= R_s i_q + L_q \frac{di_q}{dt} + \frac{\pi v}{\tau} L_d i_d + \frac{\pi v}{\tau} \psi_f \\ fe &= \frac{3\pi}{2\tau} p_n [\psi_f i_q + (L_d - L_q) i_d i_q] \end{aligned} \right\} \quad (1)$$

where u_d, u_q is the $d-q$ shaft voltage; R_s is the resistance; i_d, i_q is the $d-q$ shaft current; L_d, L_q is the $d-q$ shaft inductance; v is the speed; τ is the pole distance; ψ_f is the permanent magnet flux linkage; fe is the electromagnetic thrust; and p_n is the number of armature pole pairs.

The equation of motion of PPMLM is given by:

$$fe = M\dot{v} + Bv + f_l \quad (2)$$

where M is the mass of the moving part of the motor; B is the viscous friction coefficient; and f_l is the load.

Since the MFAC method proposed in this work is aimed at discrete nonlinear systems, Equation (2) is discretized, and the motion equation of the continuous-time system is discretized as:

$$\frac{v(k+1) - v(k)}{h} = \frac{fe(k)}{M} - \frac{f_l}{M} - \frac{B}{M}v(k) \quad (3)$$

where h is the sampling period of the system; $v(k)$ is the speed-control output of the PPMLM direct thrust control system at the moment k ; and $fe(k)$ is the control thrust input at the moment k .

After arranging Equation (3), we find:

$$v(k+1) = \left(1 - \frac{B}{M}h\right)v(k) + \frac{fe(k)}{M}h - \frac{f_l}{M}h \quad (4)$$

Remark 1. The dynamics of PPMLM motion shown in Equation (4) is obtained by Euler discretization of Equation (2), which represents the relationship between the speed output of the PPMLM and the control thrust input in each sampling period. Equation (4) does not contain a differential relationship, so it is easier to derive the relationship between the control input and output, which is the basis for the design of discrete controller that is presented later.

3. Design of the MFAC Algorithm

The control goal of this paper is to design a suitable speed controller, ensuring an accurate speed-tracking result for the PPMLM control system. In this section, the CFDL–MFAC, CFDL–MFAPC, and IESO–CFDL–MFAC speed controllers are designed.

Since the DTFC system of the PPMLM is a single-input single-output (SISO) nonlinear system, the SISO discrete-time nonlinear system follows:

$$v(k+1) = f(v(k), \dots, v(k-\sigma_v), fe(k), \dots, fe(k-\sigma_{fe})) \quad (5)$$

where $v(k) \in R$, $fe(k) \in R$, respectively, express the output and input of the system at the moment, namely the speed fed back by the PPMLM and the thrust output by the speed controller, where σ_v and σ_{fe} are two unknown positive integers.

When introducing the model-free adaptive control algorithm, two assumptions need to be made for the DTFC system of the PPMLM:

Assumption 1 [27]. The partial derivative of $f(\dots)$ shown in Equation (5) concerning $(\sigma_v + 2)$ control input thrust variable is continuous.

Assumption 2 [27]. The DTFC system of the PPMLM needs to satisfy the generalized Lipschitz condition, that is, for any $k_1 \neq k_2$, $k_1, k_2 \geq 0$, and $fe(k_1) \neq fe(k_2)$:

$$|v(k_1+1) - v(k_2+1)| \leq \chi |fe(k_1) - fe(k_2)| \quad (6)$$

where

$$v(k_i+1) = f(v(k_i), \dots, v(k_i-\sigma_v), fe(k_i), \dots, fe(k_i-\sigma_{fe})) \quad (7)$$

In the formula, $i = 1, 2$; $\chi > 0$ is a constant.

When the direct thrust control system satisfies assumptions 1 and 2, and $|\Delta fe(k)| \neq 0$, there is a pseudo partial derivative (PPD) $\varphi(k) \in R$, so that the DTFC system is changed into the compact form of model-free adaptive control (CFDL), as shown in the following formula:

$$\Delta v(k+1) = \varphi(k) \Delta fe(k) \quad (8)$$

where $\Delta v(k+1) = v(k+1) - v(k)$ is the change in speed and $\Delta fe(k) = fe(k) - fe(k-1)$ is the change in electromagnetic thrust.

Equation (8) is an equivalent dynamic linearization representation of Equation (5), where the time-varying parameter $\varphi(k)$ is the PPD of the system.

Corollary 1. According to assumption 2 and Equation (8), for any time k , there must be a time-varying parameter $\varphi(k) \in R$ called the pseudo partial derivative (PPD), which satisfies $|\varphi(k)| \leq \bar{\chi}$.

3.1. Design of the Control Algorithm Based on CFDL–MFAC

Figure 2 shows the block diagram of the CFDL–MFAC-based DTFC system of PPMLM. The control input criterion function follows:

$$J(fe(k)) = |v^*(k+1) - v(k+1)|^2 + \lambda |fe(k) - fe(k-1)|^2 \quad (9)$$

Bringing Equation (8) into Equation (9), taking the derivation of the control input $fe(k)$, and making the derivation result zero, the CFDL–MFAC control algorithm shown in Equation (10) can be obtained.

$$fe(k) = fe(k-1) + \frac{\rho \varphi(k)}{\lambda + |\varphi(k)|^2} (v^*(k+1) - v(k)) \quad (10)$$

In the formula, ρ and λ are constants greater than zero, which can make this control algorithm more general.

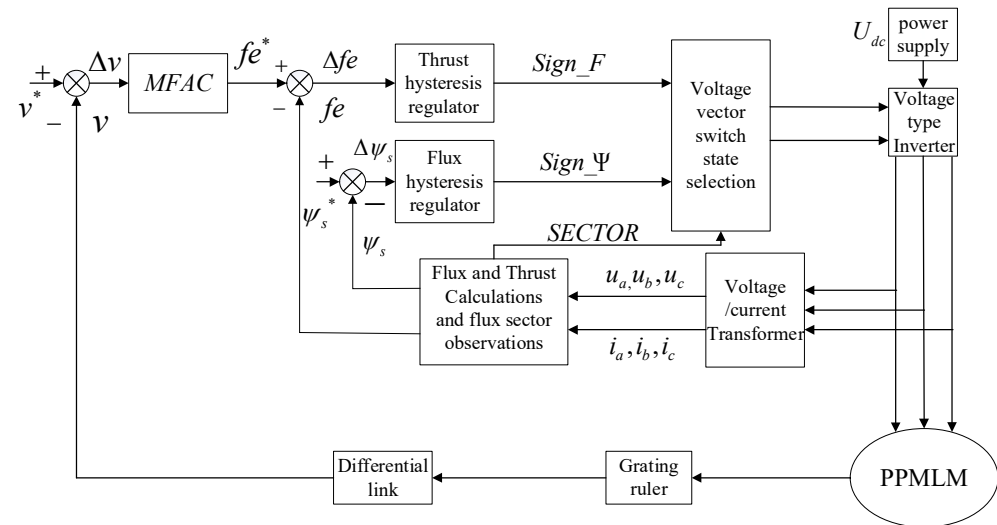


Figure 2. Block diagram of the PPMLM direct thrust force control system based on CFDL–MFAC.

To solve the pseudo partial derivative in Equation (10), the PPD estimation criterion function shown in the following equation is proposed:

$$J(\varphi(k)) = |v(k) - v(k-1) - \varphi(k)\Delta fe(k-1)|^2 + \mu|\varphi(k) - \hat{\varphi}(k-1)|^2 \quad (11)$$

Similarly, by taking the derivative of $\varphi(k)$ in Equation (11) and making it equal to zero, the following PPD estimation algorithm can be obtained:

$$\hat{\varphi}(k) = \hat{\varphi}(k-1) + \frac{\eta \Delta f e(k-1)}{\mu + \Delta f e(k-1)^2} (\Delta v(k) - \hat{\varphi}(k-1) \Delta f e(k-1)) \quad (12)$$

$$\begin{aligned} \hat{\phi}(k) = \hat{\phi}(1), \text{ if } |\hat{\phi}(k)| \leq \varepsilon \text{ or } |\Delta fe(k-1)| \leq \varepsilon, \text{ or} \\ \text{sign}(\hat{\phi}(k)) \neq \text{sign}(\hat{\phi}(1)) \end{aligned} \quad (13)$$

where $\eta \in (0, 1]$ is the step-size factor estimated for the PPD, $\mu > 0$ is the penalty factor for the amount of change in the estimated value of PPD; ε is a small number; and $\hat{\phi}(1)$ is the initial value of $\hat{\phi}(k)$.

Remark 2. Note that the PPMLM DTFC system based on CFDL–MFAC is closed-loop stable, where only the input and output data of the PPMLM DTFC system is used in the control algorithm. As such, specific mathematics of the PPMLM are not needed and used in the design of the speed controller, which significantly improves the control design flexibility.

3.2. Design of the Control Algorithm Based on CFDL–MFAPC

In this subsection, MFAC and predictive control are combined to optimize the speed-control algorithm and improve the speed-control algorithm by predicting the upcoming data, together with the control accuracy and system robustness. Figure 3 shows the block diagram of the CFDL–MFAPC-based DTFC system of PPMLM.

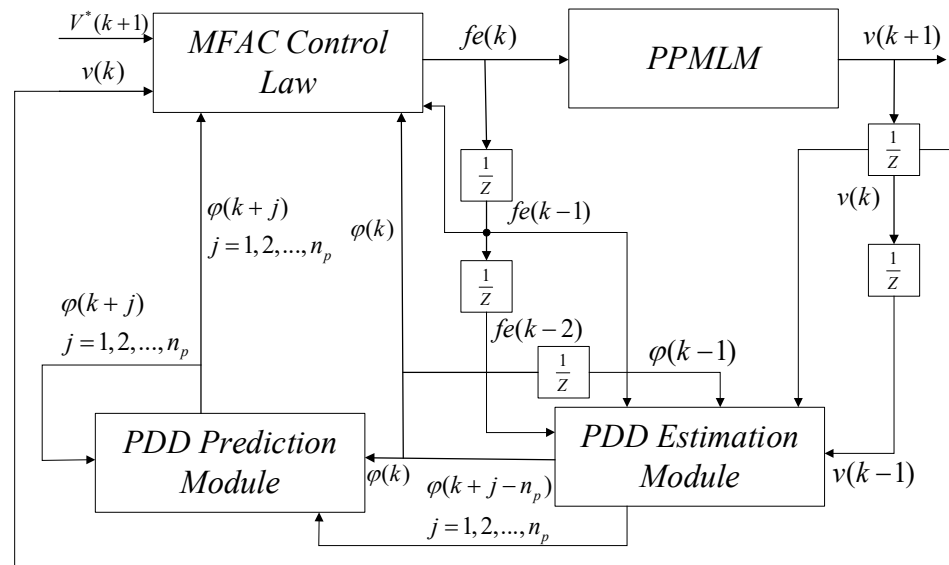


Figure 3. Structure diagram of the control algorithm based on CFDL–MFAPC.

The assumptions proposed in the previous subsection are also applicable in this subsection. First, Equation (8) is transformed into:

$$v(k+1) = v(k) + \varphi(k)\Delta fe(k) \quad (14)$$

Then, the prediction equation for a step forward can be written once according to Equation (14):

$$\left. \begin{aligned} v(k+1) &= v(k) + \varphi(k)\Delta fe(k), \\ v(k+2) &= v(k+1) + \varphi(k+1)\Delta fe(k+1) \\ &= v(k) + \varphi(k)\Delta fe(k) \\ &\quad + \varphi(k+1)\Delta fe(k+1), \\ &\vdots \\ v(k+N) &= v(k+N-1) + \varphi(k+N-1) \\ &\quad \Delta fe(k+N-1) \\ &= v(k+N-2) + \varphi(k+N-2) \\ &\quad \Delta fe(k+N-2) \\ &\quad + \varphi(k+N-1)\Delta fe(k+N-1) \\ &\vdots \\ &= v(k) + \varphi(k)\Delta fe(k) + \cdots + \\ &\quad \varphi(k+N-1)\Delta fe(k+N-1) \end{aligned} \right\} \quad (15)$$

$$\text{Make } V_N(k+1) = [v(k+1), v(k+2), \dots, v(k+N)]^T \\ \Delta Fe_N(k) = [\Delta fe(k), \Delta fe(k+2), \dots, \Delta fe(k+N-1)]^T, E(k) = [1, 1, \dots, 1]^T$$

$$\mathbf{H}(k) = \begin{bmatrix} \varphi(k) & 0 & 0 & 0 & 0 & 0 \\ \varphi(k) & \varphi(k+1) & 0 & 0 & & \\ \cdot & \cdot & \cdot & \cdot & & \cdot \\ \cdot & \cdot & \cdot & \cdot & & \cdot \\ \cdot & \cdot & \cdot & \cdot & & \cdot \\ \varphi(k) & \cdot & \cdot & \cdot & \varphi(k+N_u-1) & \\ \cdot & & & & \cdot & \cdot \\ \cdot & & & & \cdot & \cdot \\ \cdot & & & & \cdot & 0 \\ \varphi(k) & \varphi(k+1) & \cdot & \varphi(k+N_u-1) & \cdot & \varphi(k+N-1) \end{bmatrix}_{N \times N}$$

where $\mathbf{V}_N(k+1)$ is the matrix composed of the vector of step-forward prediction output by the control system; $\Delta \mathbf{F}e_N(k)$ is the control input matrix composed of the control input at the current moment k and its increment vector.

Equation (15) can be abbreviated as the following matrix form:

$$\mathbf{V}_N(k+1) = \mathbf{E}(k)v(k) + \mathbf{H}(k)\Delta \mathbf{F}e_N(k) \quad (16)$$

If $\Delta fe(k+j-1) = 0$, then Equation (16) can be changed into:

$$\mathbf{V}_N(k+1) = \mathbf{E}(k)v(k) + \hat{\mathbf{H}}(k)\Delta \mathbf{F}e_{N_u}(k) \quad (17)$$

where $\Delta \mathbf{F}e_{N_u}(k) = [\Delta fe(k), \dots, \Delta fe(k+N_u-1)]^T$, N_u is a constant controlling the time domain, then:

$$\hat{\mathbf{H}}(k) = \begin{bmatrix} \varphi(k) & 0 & 0 & 0 \\ \varphi(k) & \varphi(k+1) & 0 & 0 \\ \cdot & \cdot & \cdot & \cdot \\ \cdot & \cdot & \cdot & \cdot \\ \cdot & \cdot & \cdot & \cdot \\ \varphi(k) & \varphi(k+1) & \cdot & \cdot & \varphi(k+N_u-1) \\ \cdot & \cdot & \cdot & \cdot & \cdot \\ \cdot & \cdot & \cdot & \cdot & \cdot \\ \cdot & \cdot & \cdot & \cdot & \cdot \\ \varphi(k) & \varphi(k+1) & \cdot & \cdot & \varphi(k+N_u-1) \end{bmatrix}_{N \times N_u}$$

Consider the control criterion function given by:

$$J = [\mathbf{V}_N^*(k+1) - \mathbf{V}_N(k+1)]^T [\mathbf{V}_N^*(k+1) - \mathbf{V}_N(k+1)] + \lambda \Delta \mathbf{F}e_{N_u}^T(k) \Delta \mathbf{F}e_{N_u}(k) \quad (18)$$

where, $\mathbf{V}_N^*(k+1) = [v^*(k+1), \dots, v^*(k+N)]^T$.

Substituting Equation (17) into Equation (18), according to $\frac{\partial J}{\partial \mathbf{F}e_{N_u}(k)} = 0$, we obtain:

$$\Delta \mathbf{F}e_{N_u}(k) = [\hat{\mathbf{H}}^T(k)\hat{\mathbf{H}}(k) + \lambda \mathbf{I}]^{-1} \hat{\mathbf{H}}^T(k) [\mathbf{V}_N^*(k+1) - \mathbf{E}(k)v(k)] \quad (19)$$

Therefore, the thrust control input available at the current moment is:

$$fe(k) = fe(k-1) + \mathbf{g}^T \Delta \mathbf{F}e_{N_u}(k) \quad (20)$$

where $\mathbf{g} = [\rho, 0, \dots, 0]^T$, $\rho > 0$.

This subsection solves the partial derivative algorithm in the same way as in the previous subsection:

$$\hat{\varphi}(k) = \hat{\varphi}(k-1) + \frac{\eta \Delta fe(k-1)}{\mu + \Delta fe(k-1)^2} (\Delta v(k) - \hat{\varphi}(k-1) \Delta fe(k-1)) \quad (21)$$

In this section, $\hat{H}(k)$ needs to be predicted in advance for the value of the partial derivative at the first few moments, but the $\varphi(k+1) \cdots \varphi(k+N_u-1)$ in $\hat{H}(k)$ cannot be calculated from the I/O data of the control system at time k similar to traditional MFAC, and the estimated $\hat{\varphi}(1) \cdots \hat{\varphi}(k)$ needs to be used for the calculation. Therefore, it is necessary to use the estimated values of $\hat{\varphi}(1) \cdots \hat{\varphi}(k)$ that can be calculated to predict the unknown parameter $\varphi(k+1) \cdots \varphi(k+N_u-1)$ forward by using the multilayer hierarchical forecasting method, and then establish an autoregressive (AR) model satisfied by the estimated sequence, as shown in the following formula:

$$\hat{\varphi}(k+1) = \theta_1(k) \hat{\varphi}(k) + \theta_2(k) \hat{\varphi}(k-1) + \cdots + \theta_{np}(k) \hat{\varphi}(k-np+1) \quad (22)$$

where, make $\theta_1(k), \dots, \theta_{np}(k)$ be $\theta_i, i = 1, \dots, np$, np is the appropriate level.

$$\hat{\varphi}(k+j) = \theta_1(k) \hat{\varphi}(k+j-1) + \theta_2(k) \hat{\varphi}(k+j-2) + \cdots + \theta_{np}(k) \hat{\varphi}(k+j-np) \quad (23)$$

According to Equation (22), a general partial derivative prediction algorithm is written: where, $j = 1, \dots, N_u - 1$.

The $\theta_1(k), \dots, \theta_{np}(k)$ in the formula is composed of a matrix $\theta(k) = [\theta_1(k), \dots, \theta_{np}(k)]^T$, and the $\theta(k)$ algorithm follows:

$$\theta(k) = \theta(k-1) + \frac{\hat{\varphi}(k-1)}{\delta + \|\hat{\varphi}(k-1)\|^2} [\hat{\varphi}(k) - \hat{\varphi}^T(k-1) \theta(k-1)] \quad (24)$$

where, $\hat{\varphi}(k-1) = [\hat{\varphi}(k-1), \dots, \hat{\varphi}(k-np)]^T, \delta \in (0, 1]$.

Therefore, the control algorithm of the MFAPC of the PPMLM DTFC system is displayed in the following formula:

$$\hat{\varphi}(k) = \hat{\varphi}(k-1) + \frac{\eta \Delta fe(k-1)}{\mu + \Delta fe(k-1)^2} (\Delta v(k) - \hat{\varphi}(k-1) \Delta fe(k-1)) \quad (25)$$

$$\hat{\varphi}(k) = \hat{\varphi}(1), \text{ if } |\hat{\varphi}(k)| \leq \varepsilon \text{ or } |\Delta fe(k-1)| \leq \varepsilon \text{ or}$$

$$\text{sign}(\hat{\varphi}(k)) \neq \text{sign}(\hat{\varphi}(1)) \quad (26)$$

$$\theta(k) = \theta(k-1) + \frac{\hat{\varphi}(k-1)}{\delta + \|\hat{\varphi}(k-1)\|^2} [\hat{\varphi}(k) - \hat{\varphi}^T(k-1) \theta(k-1)] \quad (27)$$

$$\text{If } \|\theta(k)\| \geq L,$$

$$\theta(k) = \theta(1) \quad (28)$$

$$\hat{\varphi}(k+j) = \theta_1(k) \hat{\varphi}(k+j-1) + \theta_2(k) \hat{\varphi}(k+j-2) + \cdots + \theta_{np}(k) \hat{\varphi}(k+j-np) \quad (29)$$

where, $j = 1, 2, \dots, N_u - 1$.

$$\hat{\varphi}(k+j) = \hat{\varphi}(1), \text{ if } |\hat{\varphi}(k+j)| \leq \varepsilon \text{ or}$$

$$\text{sign}(\hat{\varphi}(k+j)) \neq \text{sign}(\hat{\varphi}(1)), j = 1, 2, \dots, N_u - 1 \quad (30)$$

$$\Delta Fe_{N_u}(k) = [\hat{H}^T(k) \hat{H}(k) + \lambda I]^{-1} \hat{H}^T(k) [V_N^*(k+1) - E(k)v(k)] \quad (31)$$

$$fe(k) = fe(k-1) + g^T \Delta Fe_{N_u}(k) \quad (32)$$

In the formula, ε is a small number, L is a positive constant, $\hat{H}(k)$ and $\hat{\varphi}(k+j)$ are estimates of $H(k)$ and $\varphi(k+j)$, $j = 1, \dots, N_u - 1$, $\lambda > 0$, $\mu > 0$, $\eta \in (0, 1]$, $\delta \in (0, 1]$, $\rho > 0$.

Remark 3. In the design of the MFAPC controller, the PDD parameter matrix $H(k)$ is formed by predicting the unknown PDD parameters, which reduces the sensitivity of the controller parameters. When the system is changed, the controller parameters can only be fine-tuned. The dimension of $H(k)$ is determined by the prediction step N , and the control time domain N_u is usually the same as N . With the increase in N and N_u , the larger the dimension of $H(k)$, the better the control effect and the speed-tracking performance. However, considering that the amount of calculation also increases, we select $N = N_u = 5$ in this work, which not only ensures a smooth speed-tracking curve, but also leads to a moderate amount of calculation.

3.3. Design of the Control Algorithm Based on IESO–CFDL–MFAPC

Although the control method based on CFDL–MFAPC predicts the data of the previous moments in advance, which is equivalent to amplifying the parameters in CFDL–MFAC by N times, it is less sensitive to the controller parameters than CFDL–MFAC and has superior convergence speed and tracking accuracy. Although the square control algorithm based on MFAC is not very sensitive to the parameter changes in the system mathematical model, it still causes the system to fluctuate when the load changes suddenly and the system has unknown disturbances, thereby affecting the control accuracy of the system. This subsection adds an improved extended state observer based on the CFDL–MFAPC control method described in the previous subsection, which is used to estimate the disturbance caused by the sudden load of the system and other factors, and serves as feedforward compensation in the direct thrust control system. Figure 4 shows the block diagram of the DTFC system of PPMLM based on IESO–CFDL–MFAPC.

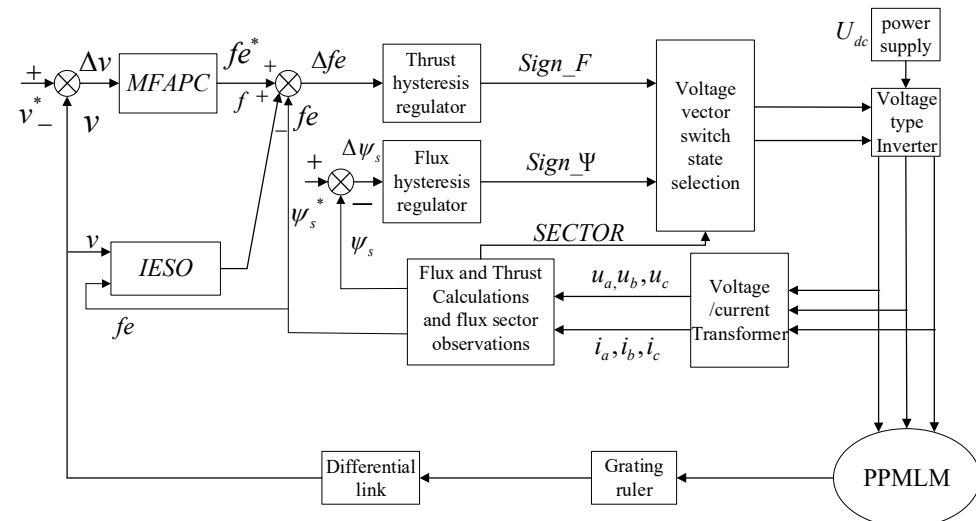


Figure 4. Block diagram of PPMLM direct thrust force control system based on IESO–CFDL–MFAPC.

The internal and external disturbance produced in the system is called the total disturbance f of the system; f is a nonlinear equation formed by the unknown disturbance of the system, and the designed extended state observer is to estimate the unknown disturbance f in the system.

Therefore, the second-order ESO equation in continuous time is designed as:

$$\left. \begin{aligned} e &= z_1 - v \\ \dot{z}_1 &= z_2 - \beta_1 fal(e, \alpha_1, \delta) + bu \\ \dot{z}_2 &= -\beta_2 fal(e, \alpha_2, \delta) \end{aligned} \right\} \quad (33)$$

$$fal(e, \alpha, \delta) = \begin{cases} \frac{e}{\delta^{\alpha-1}}, & |e| \leq \delta \\ |e|^{\alpha} \text{sign}(e), & |e| > \delta \end{cases} \quad (34)$$

where z_1 is the estimated value of the following motor speed v ; z_2 is the estimated value of the total disturbance f ; u is thrust of primary permanent magnet linear motor; β_1, β_2 is the observer gain coefficient; α_1, α_2 is the filter factor; δ is the width of the linear region; and b is a constant.

However, the speed controller designed in this paper is based on the discretized control algorithm, and then the second-order ESO is represented by the discretization, as shown in the following formula:

$$\left. \begin{aligned} e(k) &= z_1(k) - v(k) \\ z_1(k+1) &= z_1(k) + h(z_2(k) - \beta_1 fal(e, \alpha_1, \delta) + bu(k)) \\ z_2(k+1) &= z_2(k) - h\beta_2 fal(e, \alpha_2, \delta) \end{aligned} \right\} \quad (35)$$

where $z_1(k)$ is the evaluated value of the following motor speed v and $z_2(k)$ is the unknown total disturbance $f(k)$ evaluated for the system.

The total input of the PPMLM direct thrust control system then becomes:

$$U = fe(k) + f(k) \quad (36)$$

For the problem that the control accuracy of the second-order ESO is not ideal when the error is large, the fal function in the formula is correspondingly improved, and the expression for this follows:

$$fal(e, \alpha, \delta) = \begin{cases} \frac{e}{\delta^{\alpha-1}}, & |e| \leq \delta \\ |e|^{\alpha} \tanh(e), & |e| > \delta \end{cases} \quad (37)$$

After the hyperbolic tangent function is applied to the fal function, the speed tracking can converge faster and the control accuracy is higher when the system is disturbed greatly.

Remark 4 . Because the hyperbolic tangent function is used in the fal function, the transition process of the estimated disturbance is smoother. It should be noted that the output $f(k)$ of the IESO is the lumped disturbance of the system, while the control input is compensated directly without identifying the disturbance of the system.

3.4. Closed-Loop Stability Proof of the PPMLM Direct Thrust Control System Based on IESO-CFDL-MFAPC

For proving the closed-loop stability of the PPMLM DTFC system, the following assumptions are given:

Assumption 3 [33]. For a given desired velocity $v^*(k+1)$ of the PPMLM in the direct thrust control system, there is always a bounded $fe(k)$ that can make the speed output of the PPMLM direct thrust control system equal to $v^*(k+1)$.

Assumption 4 [33]. At any moment k and $\Delta fe(k) \neq 0$, the sign of $\varphi(k)$ for the system can be kept unchanged, that is, to satisfy $\varphi(k) > \varepsilon > 0$, or $\varphi(k) < -\varepsilon$, where ε is a small number.

Corollary 2. According to Assumption 2 and Equation (8), for any time k , there must be a time-varying PPD $\varphi(k) \in \mathbb{R}$ that satisfies $|\varphi(k)| \leq \bar{\chi}$.

Theorem. For the nonlinear PPMLM direct thrust control system, under the condition that the assumptions above are satisfied and when $v^*(k+1) = v^* = \text{const}$, then there is a positive number $\lambda_{\min} > 0$, such that when $\lambda > \lambda_{\min}$:

- (1) The error $e(k)$ of the system speed is monotonically convergent, that is, $\lim_{k \rightarrow \infty} |v^* - v(k+1)| = 0$.
- (2) The closed-loop system of direct thrust control is bounded-input bounded-output (BIBO) stable, that is, the output speed-control sequence $\{v(k)\}$ and the input thrust control sequence $\{fe(k)\}$ are bounded.

Proof. If the speed controller designed in this paper satisfies the condition $|\hat{\varphi}(k)| \leq \varepsilon$ or $|\Delta fe(k-1)| \leq \varepsilon$, or $\text{sign}(\hat{\varphi}(k)) \neq \text{sign}(\hat{\varphi}(1))$, then the pseudo partial derivative $\hat{\varphi}(k)$ is obviously bounded. \square

In addition to the cases above, we define $e_\varphi(k) = \hat{\varphi}(k) - \varphi(k)$ as the error of partial derivative estimation. Subtracting $\varphi(k)$ from both ends of the parameter estimation algorithm (Equation (25)) at the same time and combining with Equation (14), we obtain:

$$\begin{aligned} e_\varphi(k) &= e_\varphi(k-1) - \Delta\varphi(k) + \frac{\eta\Delta fe(k-1)}{\mu + \Delta fe(k-1)^2} (\Delta v(k) - \hat{\varphi}(k-1)\Delta fe(k-1)) \\ &= (1 - \frac{\eta\Delta fe(k-1)^2}{\mu + \Delta fe(k-1)^2}) e_\varphi(k-1) - \Delta\varphi(k) \end{aligned} \quad (38)$$

From the conclusion $|\varphi(k)| \leq \bar{\chi}$ in the corollary, $|\varphi(k-1) - \varphi(k)| \leq 2\bar{\chi}$ is known. By deducting the absolute values on both sides of the Equation (38), we obtain:

$$\begin{aligned} |e_\varphi(k)| &\leq \left| 1 - \frac{\eta\Delta fe(k-1)^2}{\mu + \Delta fe(k-1)^2} \right| |e_\varphi(k-1)| \\ &\quad + |\Delta\varphi(k)| \leq \left| 1 - \frac{\eta\Delta fe(k-1)^2}{\mu + \Delta fe(k-1)^2} \right| |e_\varphi(k-1)| + 2\bar{\chi} \end{aligned} \quad (39)$$

Since $\mu > 0, \eta \in (0, 1]$, there is a constant p , such that the following formula holds:

$$0 < 1 - \frac{\eta\Delta fe(k-1)^2}{\mu + \Delta fe(k-1)^2} \leq p < 1 \quad (40)$$

Using Equations (39) and (40), we can obtain:

$$\begin{aligned} |e_\varphi(k)| &\leq p|e_\varphi(k-1)| + 2\bar{\chi} \leq p^2|e_\varphi(k-2)| + 2p\bar{\chi} + 2\bar{\chi} \\ &\leq \dots \leq p^{k-1}|e_\varphi(1)| + \frac{2\bar{\chi}}{1-p}. \end{aligned} \quad (41)$$

Equation (41) shows that $e_\varphi(k)$ is bounded. Additionally, because $\varphi(k)$ is bounded, we can show that $\hat{\varphi}(k)$ is bounded, and from Equations (27)–(30), it can be concluded that $\hat{\varphi}(k+j)$ is bounded.

By defining the tracking error of the system as $e(k+1) = v^* - v(k+1)$ and bringing Equation (14) into the tracking error equation, and further using Equations (31) and (32), we obtain:

$$\begin{aligned} e(k+1) &= v^* - v(k+1) \\ &= v^* - v(k) - \varphi(k)\Delta fe(k) \\ &= (1 - \varphi(k)(g^T(\hat{H}^T(k)\hat{H}(k) + \lambda I)^{-1}\hat{H}^T(k)E(k)))(v^* - v(k)) \end{aligned} \quad (42)$$

Calculating the absolute values on both sides of Equation (42) yields:

$$|e(k+1)| \leq \left| 1 - \varphi(k)(g^T(\hat{H}^T(k)\hat{H}(k) + \lambda I)^{-1}\hat{H}^T(k)E(k)) \right| |e(k)| \quad (43)$$

Let $Q = (\hat{H}^T(k)\hat{H}(k) + \lambda I)$, where $\hat{H}^T(k)\hat{H}(k)$ is a positive semidefinite matrix; if $\lambda > 0$, both Q and Q^{-1} are positive definite matrices.

Then, by $Q^{-1} = \frac{Q^*}{\det(Q)}$,
 where $Q^* = \begin{bmatrix} Q_{11} & \cdots & Q_{N_u 1} \\ \vdots & \ddots & \vdots \\ Q_{1N_u} & \cdots & Q_{N_u N_u} \end{bmatrix}$ is the adjoint matrix of the matrix Q , and Q_{ij} is the algebraic cofactor of Q , the following formula holds:

$$\begin{aligned} & g^T (\hat{H}^T(k) \hat{H}(k) + \lambda I)^{-1} \hat{H}^T(k) E(k) \\ &= g^T Q^{-1} \hat{H}^T(k) E(k) \\ &= g^T \frac{Q^*}{\det(Q)} \hat{H}^T(k) E(k) \\ &= \frac{N \hat{\phi}(k) Q_{11}}{\det(Q)} + \frac{(N-1) \hat{\phi}(k+1) Q_{21}}{\det(Q)} + \dots + \frac{(N-N_u+1) \hat{\phi}(k+N_u-1) Q_{N_u 1}}{\det(Q)} \end{aligned} \quad (44)$$

Since $\hat{\phi}(k)$ is known to be bounded at any time k , Equation (44) is bounded and the upper bound is a constant independent of k .

Because Q is a positive definite matrix, $\det(Q) > 0$ is a polynomial of order N_u with the leading coefficient of λ being 1. $Q_{11} > 0$ is a polynomial of order $(N_u - 1)$ with the leading coefficient of λ being 1. $Q_{i1} (i = 2, 3, \dots, N_u)$ is a polynomial of order $(N_u - 2)$ with the leading coefficient of λ being 1. Thus, there is $\lambda_{\min} > 0$ such that when $\lambda \geq \lambda_{\min}$, the sign of Equation (44) is the same as $\frac{Q_{11}}{\det(Q)}$, and further, there is a constant q , such that:

$$0 < 1 - \varphi(k) (g^T (\hat{H}^T(k) \hat{H}(k) + \lambda I)^{-1} \hat{H}^T(k) E(k)) \leq q < 1 \quad (45)$$

From Equations (43) and (45), we know that:

$$|e(k+1)| \leq q|e(k)| \leq \dots \leq q^k |e(1)| \quad (46)$$

Therefore, $\lim_{k \rightarrow \infty} |e(k+1)| = 0$.

Since $v^*(k)$ is a bounded constant, it follows that the sequence $\{v(k)\}$ is also bounded. Using Equations (31) and (32), we obtain:

$$|\Delta f e(k)| \leq \left| g^T (\hat{H}^T(k) \hat{H}(k) + \lambda I)^{-1} \hat{H}^T(k) E(k) \right| |e(k)| \leq \Gamma |e(k)| \quad (47)$$

where Γ is a bounded constant.

Further, we have:

$$\begin{aligned} |f e(k)| &\leq |\Delta f e(k)| + |\Delta f e(k-1)| + \dots + |\Delta f e(2)| + |f e(1)| \\ &\leq \Gamma (|e(k)| + |e(k-1)| + \dots + |e(2)|) + |f e(1)| \\ &\leq \Gamma (q^{k-1} |e(1)| + \dots + q |e(1)|) + |f e(1)| \\ &\leq \Gamma \frac{q |e(1)|}{1-q} + |f e(1)| \end{aligned} \quad (48)$$

Equation (48) shows that the sequence $\{f e(k)\}$ is also bounded.

Furthermore, it can be shown that the PPMLM DTFC system based on CFDL-MFAPC is closed-loop stable.

Considering that β_1, β_2 are the observer gain coefficients and h is the sampling period, when IESO selects an appropriate observation gain and sampling period, the estimated value $z_2(k)$ of the total disturbance converges to $f(k)$ in a finite time k , namely, $f(k) < \zeta$, where ζ is a constant [37], and the control law $f e(k)$ is bounded. Then, from Equation (36), we can see that the total control law $U(k)$ is also bounded.

Therefore, the PPMLM DTFC system based on IESO-CFDL-MFAPC is also closed-loop stable.

4. Simulation Verification

The main parameters of the PPMLM in the simulation are displayed in Table 1.

Table 1. Parameters of the PPMLM.

Parameter	Symbol	Unit	Value
Motor quality	M	kg	15.5
Coefficient of viscous friction	B	kg/s	0.1
Primary resistance	R	Ω	1.8
Permanent magnet pole pitch	τ	mm	45
Permanent magnet flux linkage	ψ_f	wb	0.28
Armature pole pairs	p_n	-	4
d-axis inductance	L_d	mH	2.7
q-axis inductance	L_d	mH	2.7
DC power supply	U_{dc}	V	310

To verify the effectiveness of the IESO–CFDL–MFAPC scheme, the traditional PI controller and the control algorithms based on CFDL–MFAC, CFDL–MFAPC, and IESO–CFDL–MFAPC are compared. When running at a speed of 100 N, the PPMLM starts with 100 N load, suddenly adds 100 N load at 0.65 s, and suddenly reduces 50 N load at 1.3 s to obtain the speed curves of four different controllers under disturbance changes. After repeated trial and error debug simulation, the optimal parameters of each controller and the optimal speed curve under the disturbance are finally obtained.

The sampling time of the control system in the simulation is set as 0.1 ms. The parameters and initial values of the four controllers are displayed in Tables 2 and 3:

Table 2. Parameters of the four control algorithms.

IESO–MFAPC		ESO–MFAPC		MFAPC		MFAC		PI	
λ	0.4	λ	0.4	λ	1.5	λ	0.01	K_p	1×10^3
ρ	1200	ρ	1000	ρ	1100	ρ	3.5	K_i	1×10^5
η	0.1	η	0.1	η	0.1	η	0.1	-	-
μ	1×10^{-6}	μ	1×10^{-6}	μ	1×10^{-6}	μ	1×10^{-6}	-	-
δ	1	δ	1	δ	1	-	-	-	-
ε	1×10^{-3}	ε	1×10^{-3}	ε	1×10^{-3}	-	-	-	-
N	5	N	5	N	5	-	-	-	-
N_u	5	N_u	5	N_u	5	-	-	-	-
np	3	np	3	n_p	3	-	-	-	-
β_1	1×10^5	β_1	1×10^5	-	-	-	-	-	-
β_2	4.55×10^5	β_2	3.45×10^5	-	-	-	-	-	-
α_1	0.5	α_1	0.5	-	-	-	-	-	-
α_2	0.25	α_2	0.25	-	-	-	-	-	-
b	7	b	6	-	-	-	-	-	-

Table 3. Initial parameter values for the four control algorithms.

IESO –MFAPC	ESO–MFAPC	MFAPC	MFAC	PI
$\varphi(1) = 0.5$ $\varphi(1) = \varphi(2) = \varphi(3) = \varphi(4)$ $= \varphi(5) = 0.5$ $\theta(1) = [0.5 \ 0.6 \ 0.7]$ $L = 10$	The initial value is the same as that of IESO	The initial value is the same as that of IESO	$\varphi(1) = 0.5$	-

Figures 5 and 6 show the speed-tracking curve and error curves of the four control algorithms under a sudden load, respectively. It can be seen from Figure 5 that the control effect of IESO–CFDL–MFAPC is better than the other control methods in terms of overshoot, convergence speed, error accuracy, and antidisturbance.

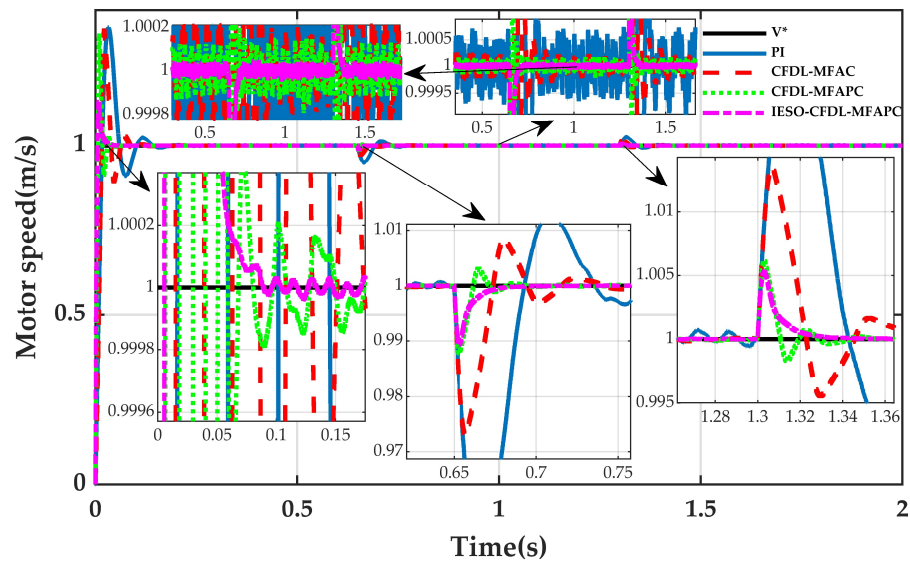


Figure 5. Speed curve for the four control algorithms under sudden load.

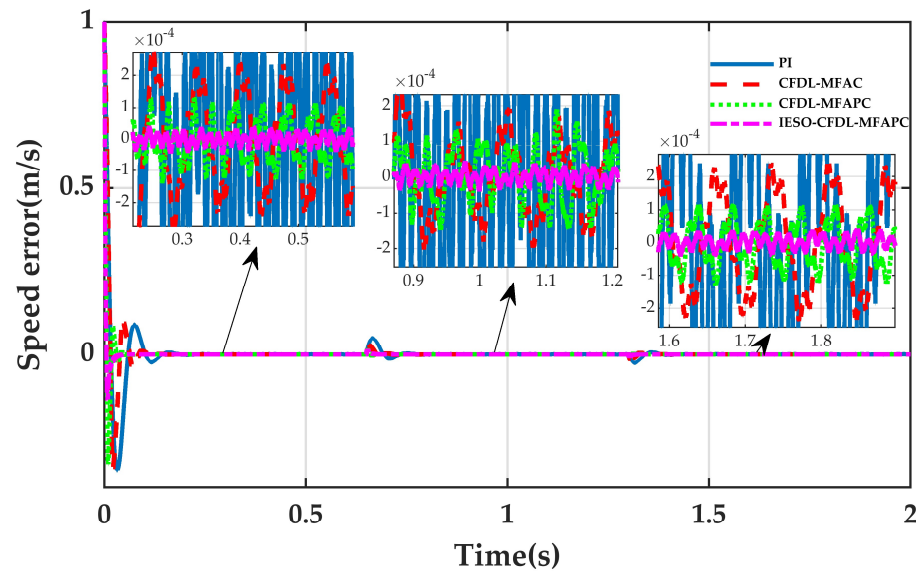


Figure 6. Speed-tracking error curves for the four control algorithms under sudden load.

Figure 7 shows that the improved ESO can ensure faster convergence and smaller speed error. When the disturbance is added, both the overshoot of the IESO and the speed error after the steady state are smaller, which indicates that the IESO has a faster convergence effect and stronger robustness.

To show the performance comparison quantitatively among the four controllers, the following root mean square error (RMSE) and maximum error (MAXE) values are selected:

$$RMSE(e(k)) = \sqrt{\frac{1}{G} \sum_{i=1}^G e(k)^2} \quad (49)$$

$$MAXE(e(k)) = \max(|e(k)|) \quad (50)$$

where $e(k)$ is the error value between each control method and the expected speed after entering a steady state, and G is the number of error samples. Three periods are considered: (i) Period 1: after startup with 100 N load; (ii) Period 2: after sudden addition of 100 N load;

(iii) Period 3: sudden reduction of 50 N load. The quantitative indicators of the four control algorithms are shown in Table 4:

Table 4. Quantitative index of four algorithms when the load changes.

Controller	Disturbance	Root Mean Square Error	Maximum Error
PI	Start with 100 N load	3.4286×10^{-4}	6.8789×10^{-4}
	Sudden 100 N load	3.1952×10^{-4}	6.4449×10^{-4}
	Sudden drop of 50 N load	4.1426×10^{-4}	9.0252×10^{-4}
MFAC	Start with 100 N load	1.4326×10^{-4}	2.3843×10^{-4}
	Sudden 100 N load	1.0365×10^{-4}	1.9340×10^{-4}
	Sudden drop of 50 N load	1.4080×10^{-4}	2.3835×10^{-4}
MFAPC	Start with 100 N load	6.9372×10^{-5}	1.3078×10^{-4}
	Sudden 100 N load	8.0155×10^{-5}	1.9047×10^{-4}
	Sudden drop of 50 N load	7.0799×10^{-5}	1.1364×10^{-4}
IESO–MFAPC	Start with 100 N load	1.8293×10^{-5}	3.7948×10^{-5}
	Sudden 100 N load	1.7799×10^{-5}	3.6790×10^{-5}
	Sudden drop of 50 N load	1.7812×10^{-5}	3.3845×10^{-5}

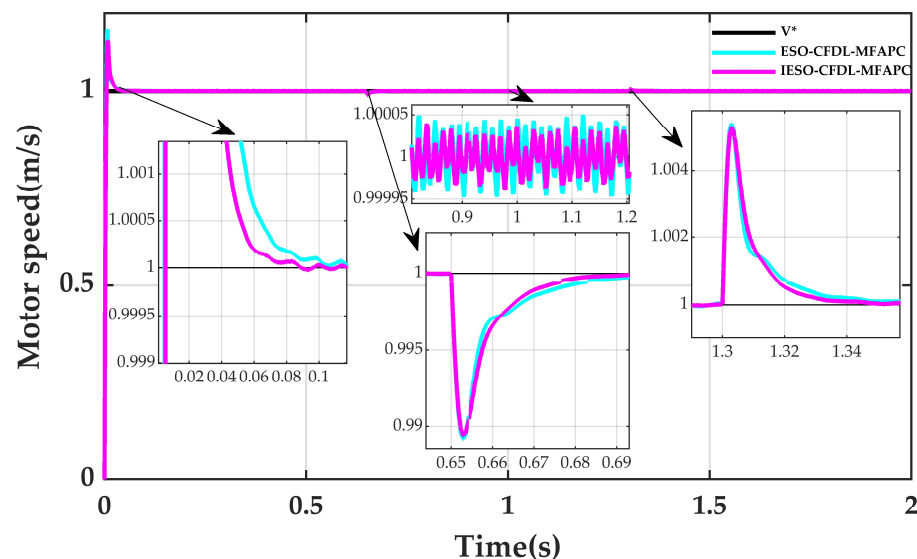


Figure 7. Speed comparison before and after ESO improvement.

From the speed comparison curves of the four control algorithms shown in Figure 5, we observe that the IESO–CFDL–MFAPC converges to the desired speed curve within 0.09 s after the PPMLM starts with a 100 N load, and only has a rapid and stable convergence after an overshoot of 0.131 m/s. The CFDL–MFAPC converges within 0.15 s after an overshoot of 0.3325 m/s, and the CFDL–MFAC without the optimization of the prediction algorithm converges within 0.2 s after an overshoot of 0.3405 m/s. The PI controller converges in 0.265 s after an overshoot of 0.35 m/s occurs.

Combined with the data in Table 4, it can be clearly shown that the control effect based on IESO–CFDL–MFAPC is the best, and the speed-tracking error of this control algorithm in the steady state after the system starts with a load of 100 N is obviously better than other three control methods.

In summary, the proposed IESO–CFDL–MFAPC shows the best speed-tracking accuracy, faster convergence speed, and stronger robustness when compared with other three control methods.

To further verify the effectiveness of the proposed method, a load of 100 N is suddenly added at 0.65 s, and a load of 50 N is suddenly dropped at 1.3 s. The proposed control

converges at 0.06 s after a drop of 0.0106 m/s at 0.65 s, while converging to the desired velocity value in 0.06 s after a rise of 0.0053 m/s occurs in 1.3 s. The CFDL-MFAPC converges to the desired velocity value in 0.07 s after a drop of 0.0122 m/s at 0.65 s, and converges in 0.062 s after a rise of 0.0061 m/s at 1.3 s. The CFDL-MFAC converges to the desired velocity value in 0.13 s after a drop of 0.0269 m/s at 0.65 s, and converges in 0.12 s after a rise of 0.0136 m/s at 1.3 s. The PI controller converges to the desired speed value in 0.16 s after a drop of 0.049 m/s in 0.65 s, and converges in 0.14 s after a rise of 0.0248 m/s in 1.3 s.

It can be seen that the proposed control shows smaller overshoot, faster convergence speed, and higher tracking accuracy, and more importantly, converges to the desired speed with a smooth curve after adding disturbance, while other three control algorithms are not as good as the proposed control, exhibiting overshoot in the opposite direction. The reasons follow: (i) After the prediction algorithm is combined with MFAPC, the convergence speed and the error accuracy are improved. (ii) By using the IESO, not only can the convergence speed of the system be improved, but also the tracking accuracy and robustness are both improved in the case of sudden disturbance.

Figure 8 shows the load variation curve, while Figure 9 depicts the thrust curve of a sudden load applied by the four control algorithms. It can be clearly seen that the thrust fluctuations of the control methods based on CFDL-MFAC, CFDL-MFAPC, and IESO-CFDL-MFAPC are all about $-5\sim 5$ N. It can be seen from Table 5 that the thrust fluctuation of IES-CFDL-MFAPC is slightly larger than that of the other two control algorithms. However, the three control algorithms have little difference in thrust fluctuation, which indicates that the proposed model-free adaptive control method can reduce the thrust fluctuation of the PPMLM. Moreover, the thrust curve based on the IESO-CFDL-MFAPC control has a faster and better convergence effect. The other two control algorithms have reverse thrust fluctuation in the process of convergence. Furthermore, the thrust fluctuation of the traditional PI controller is about $-40\sim 40$ N, indicating the worst performance of PI control. In conclusion, the control method based on IESO-CFDL-MFAPC has a better effect on the thrust curve. Clearly, the proposed control can be stabilized in the vicinity of the expected thrust much faster, and effectively improves the impact of thrust fluctuations caused by the thrust hysteresis regulator and exhibits strong antidisturbance capability.

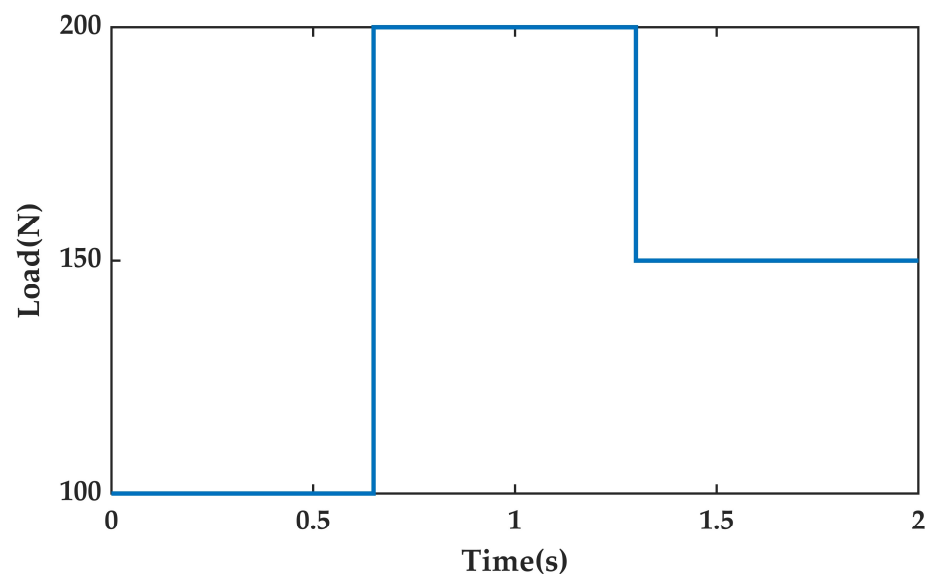


Figure 8. Load variation curve.

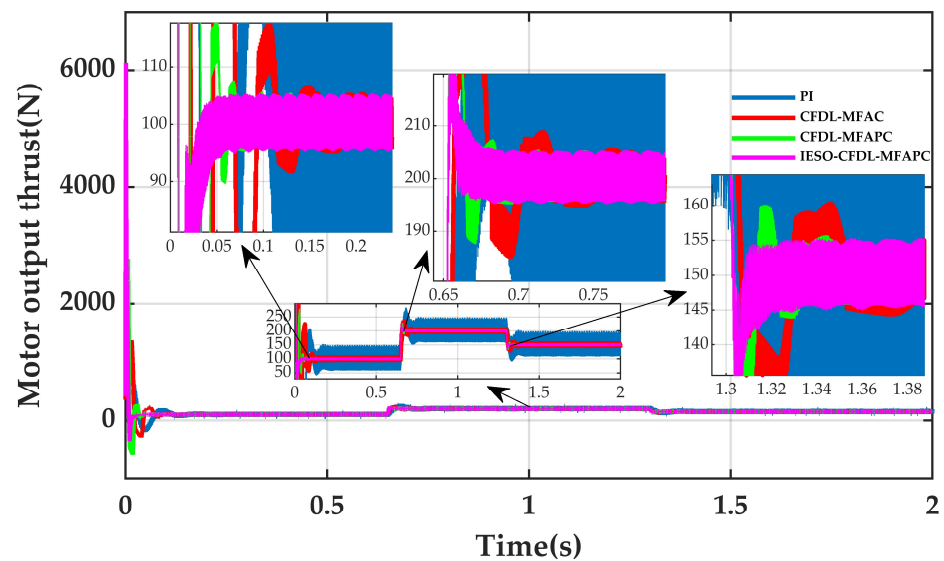


Figure 9. Thrust curve of a sudden load applied by the four control algorithms.

Table 5. Thrust fluctuation quantity index of three control algorithms under load change.

Controller	Disturbance	Root Mean Square Error	Maximum Error
MFAC	Start with 100 N load	2.0649	5.2132
	Sudden 100 N load	2.0494	5.1139
	Sudden drop of 50 N load	2.0628	5.2103
MFAPC	Start with 100 N load	2.0609	5.1443
	Sudden 100 N load	2.0471	5.3514
	Sudden drop of 50 N load	2.0515	5.1293
IESO–MFAPC	Start with 100 N load	2.0893	5.3546
	Sudden 100 N load	2.0758	5.3908
	Sudden drop of 50 N load	2.0864	5.3667

Further, it can be seen from Figures 10 and 11 that the three-phase current curve of the PPMLM under the PI controller indicates that the three-phase current distortion degree is very high, while the three-phase current curve distortion under the proposed control is significantly improved and the recovery speed is faster.

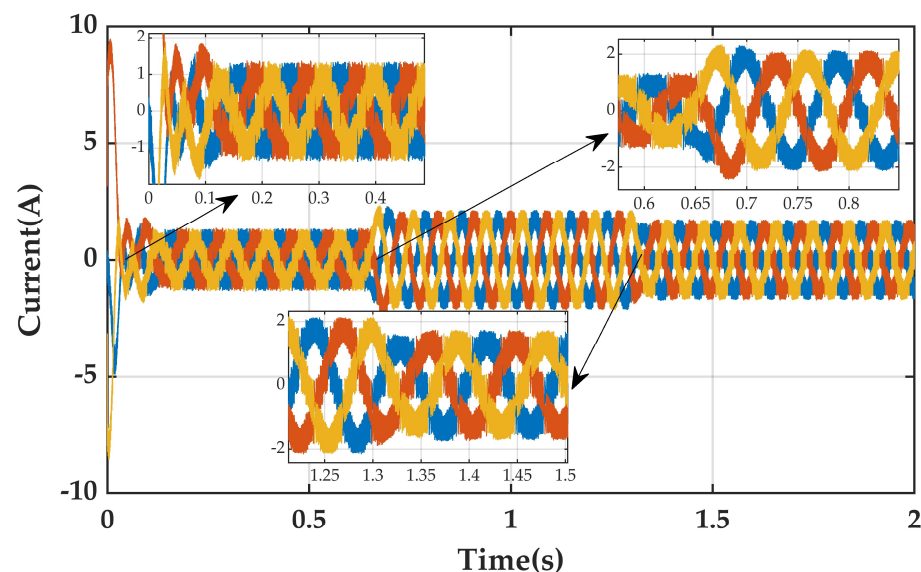


Figure 10. Three-phase current change curve of the PI controller.

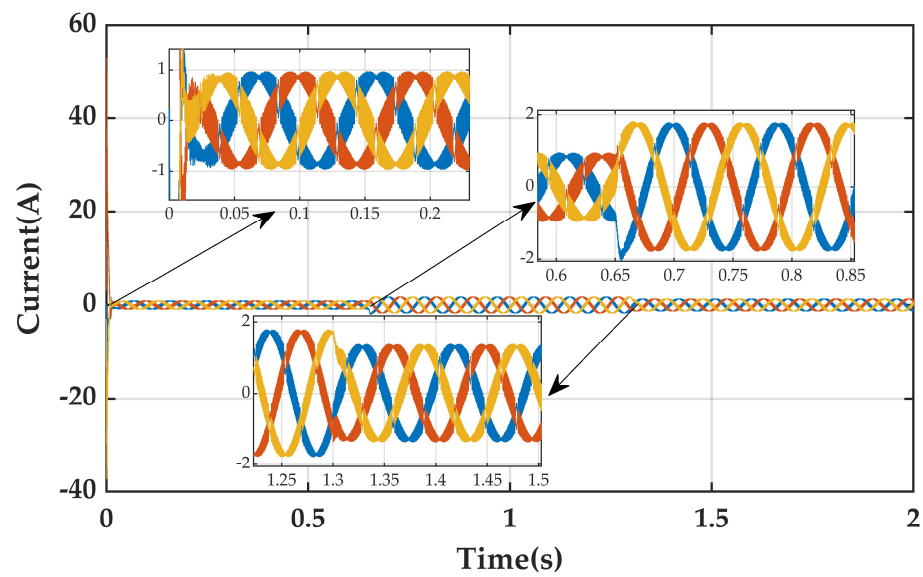


Figure 11. Three-phase current change curve of the IESO–CFDL–MFAPC controller.

Figures 12 and 13 show the flux track of the PI control and proposed control, respectively. We can clearly see that although the flux linkage of the PI controller and the IESO–CFDL–MFAPC controller is close to an ideal circle, the flux linkage based on the proposed control has smaller pulsation, which indicates that the influence of the flux fluctuation caused by the flux linkage hysteresis regulator is reduced to a certain extent.

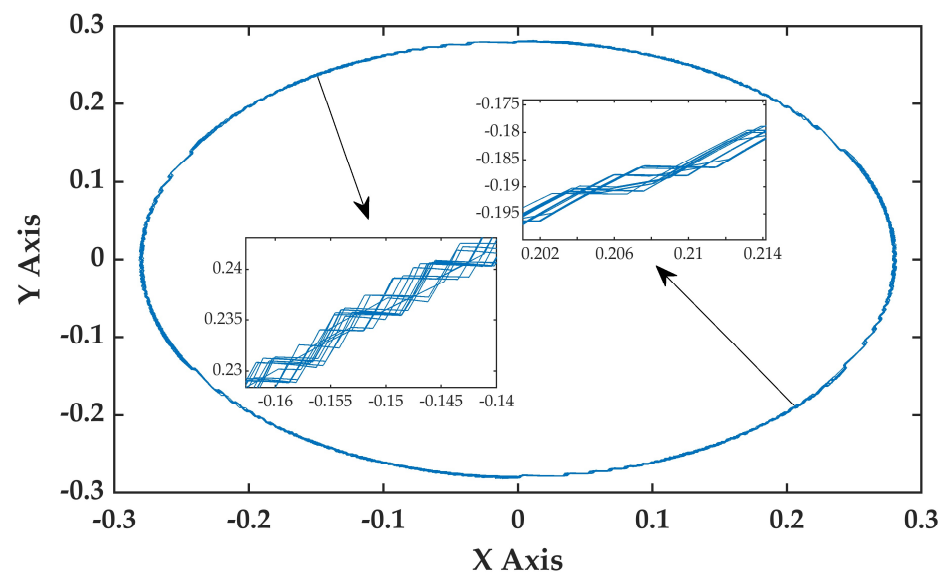


Figure 12. Flux track of the PI controller.

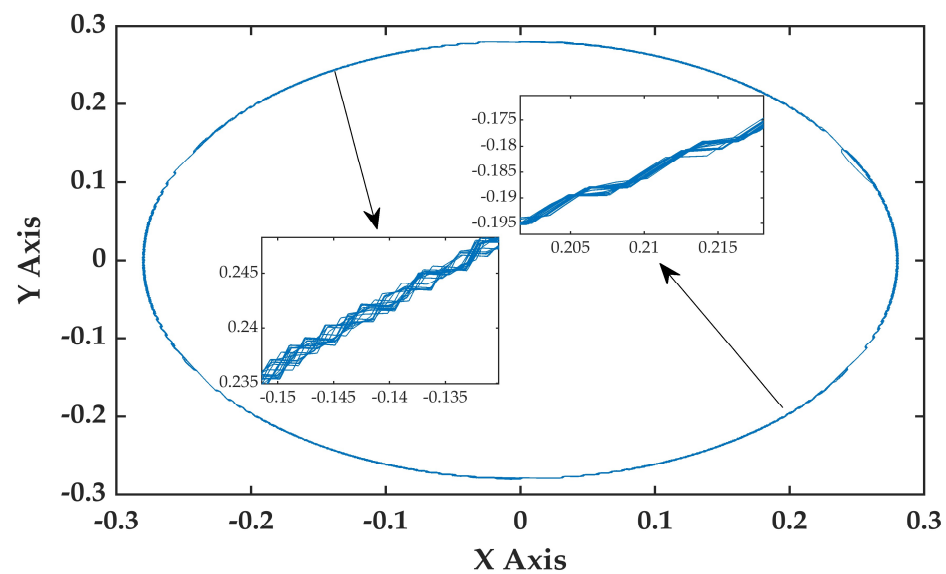


Figure 13. Flux track of the IESO–CFDL–MFAPC controller.

5. Conclusions

In this paper, a control algorithm based on IESO–CFDL–MFAPC technique is proposed to optimize the speed loop in the PPMLM direct thrust control system. The MFAC approach is first developed in the PPMLM direct thrust control system, which does not require the mathematical model of the PPMLM. It is shown that when compared with the traditional MFAC method, the MFAPC makes up for the shortcomings of the traditional MFAC and improves the speed-tracking performance by predicting the future data. Using the proposed control approach, not only can the speed-tracking performance of the PPMLM be improved, but also the disturbance in the system can be estimated in real time. As such, the influence of the system disturbance on the speed-control accuracy can be effectively compensated, which improves the antidisturbance ability and the robustness of the system. Note that in terms of the thrust fluctuation, the three model-free adaptive control methods developed in this paper have good inhibition effect on thrust fluctuation compared with the traditional PI controller, while the control method based on IESO–CFDL–MFAPC shows better speed tracking and robustness performance than other two comparable model-free adaptive control methods.

Author Contributions: Investigation, Z.X. and W.H.; Methodology, X.W. and S.Y.; Project administration, C.Q. and Y.W.; Software, S.Y.; Writing—original draft, X.W. and S.Y.; Writing—review & editing, S.Y. and H.W. All authors have read and agreed to the published version of the manuscript.

Funding: This work is supported in part by the National Natural Science Foundation of China under grant 51777127; Liaoning Natural Science Foundation under grant 2020-MS-240; Shenyang Young and Middle-aged Scientific and Technological Innovation Talents under grant RC200192; and Liaoning Provincial Department of Education Scientific Research Project under grant LJKZ1085.

Institutional Review Board Statement: Not applicable.

Informed Consent Statement: Not applicable.

Conflicts of Interest: The authors declare no conflict of interest.

References

1. Lyu, G. Review of the Application and Key Technology in the Linear Motor for the Rail Transit. *Proc. CSEE* **2020**, *40*, 5665–5675.
2. Huang, S.; Ching, T.W.; Li, W.; Deng, B. Overview of linear motors for Transportation applications. In Proceedings of the 2018 IEEE 27th International Symposium on Industrial Electronics (ISIE), Cairn, Australia, 13–15 June 2018; pp. 150–154.
3. Boldea, I.; Tutelea, L.N.; Xu, W.; Marcello, P. Linear electric machines, drives, and MAGLEVs: An overview. *IEEE Trans. Ind. Electron.* **2018**, *65*, 7504–7515. [[CrossRef](#)]

4. Wang, W.; Feng, Y.; Shi, Y.; Cheng, M.; Hua, W.; Wang, Z. Direct Thrust Force Control of Primary Permanent-Magnet Linear Motors with Single DC-Link Current Sensor for Subway Applications. *IEEE Trans. Power Electron.* **2019**, *35*, 1365–1376. [[CrossRef](#)]
5. Wang, W.; Feng, Y.; Shi, Y.; Cheng, M.; Hua, W.; Wang, Z. Fault-tolerant control of primary permanent-magnet linear motors with single-phase current sensor for subway applications. *IEEE Trans. Power Electron.* **2019**, *34*, 10546–10556. [[CrossRef](#)]
6. Karimi, H.; Vaez-Zadeh, S.; Salmasi, F.R. Combined vector and direct thrust control of linear induction motors with end effect compensation. *IEEE Trans. Energy Convers.* **2015**, *31*, 196–205. [[CrossRef](#)]
7. Zhao, X.; Jin, Y.; Wang, L. Adaptive RBFNN backstepping control for PMLSM servo system. *Electr. Mach. Control* **2020**, *24*, 149–157.
8. Hu, Y.; Wang, H.; He, S.; Zheng, J.; Ping, Z.; Shao, K.; Cao, Z.; Man, Z. Adaptive Tracking Control of an Electronic Throttle Valve Based on Recursive Terminal Sliding Mode. *IEEE Trans. Veh. Technol.* **2021**, *70*, 251–262. [[CrossRef](#)]
9. Zhang, J.; Wang, H.; Ma, M.; Yu, M.; Yazdani, A.; Chen, L. Active Front Steering-based Electronic Stability Control for Steer-by-Wire Vehicles via Terminal Sliding Mode and Extreme Learning Machine. *IEEE Trans. Veh. Technol.* **2020**, *69*, 14713–14726. [[CrossRef](#)]
10. Jin, X.; Zhao, Y.; Wang, H.; Zhao, Z.; Dong, X. Adaptive fault-tolerant control of mobile robots with actuator faults and unknown parameters. *IET Control Theory Appl.* **2019**, *13*, 1665–1672. [[CrossRef](#)]
11. Yeam, T.; Lee, D. Design of Sliding-Mode Speed Controller with Active Damping Control for Single-Inverter Dual-PMSM Drive Systems. *IEEE Trans. Power Electron.* **2021**, *36*, 5794–5801. [[CrossRef](#)]
12. Zhao, X.; Liu, C.; Zhu, G. Adaptive nonlinear sliding mode control for permanent magnet linear synchronous motor. *Electr. Mach. Control* **2020**, *24*, 39–47.
13. Zhao, X.; Zhao, J. Complementary Sliding Mode Variable Structure Control for Permanent Magnet Linear Synchronous Motor. *Proc. CSEE* **2015**, *35*, 2552–2557.
14. Zhao, X.; Ji, X.; Wang, H. Time delay adaptive integral sliding mode control for permanent magnet linear synchronous motor. *Electr. Mach. Control* **2020**, *24*, 44–50.
15. Chen, X.; Zhao, W.; Ji, J.; Tao, T.; Xue, R. Model Predictive Current Control of Double-Side Linear Vernier Permanent Magnet Machines Considering End Effect. *Trans. China Electrotech. Soc.* **2019**, *34*, 49–57.
16. Li, Z.; An, J.; Xiao, Y.; Zhang, Q.; Sun, H. Design of Model Predictive Control System for Permanent Magnet Synchronous Linear Motor Based on Adaptive Observer. *Trans. China Electrotech. Soc.* **2021**, *36*, 1190–1200.
17. Carlet, P.G.; Favato, A.; Bolognani, S.; Dörfler, F. Data-Driven Continuous-Set Predictive Current Control for Synchronous Motor Drives. *IEEE Trans. Power Electron.* **2022**, *37*, 6637–6646. [[CrossRef](#)]
18. Zhang, J.; Wang, H.; Cao, Z.; Zheng, J.; Yu, M.; Yazdani, A.; Shahnia, F. Fast nonsingular terminal sliding mode control for permanent magnet linear motor via ELM. *Neural Comput. Appl.* **2019**, *32*, 14447–14457. [[CrossRef](#)]
19. Zhao, X.; Wu, W.; Zhu, G. Varying mass estimation and disturbance compensation for permanent magnet linear servo system based on 7th-order EKF. *Electr. Mach. Control* **2020**, *24*, 79–85.
20. Zhao, X.; Wu, W.; Zhu, G. Method of PMLSM servo system long-term stable operation based on periodic learning disturbance observer. *Electr. Mach. Control* **2018**, *22*, 110–116.
21. Shen, M.; Ma, Y.; Park, J.H.; Wang, Q. Fuzzy Tracking Control for Markov Jump Systems With Mismatched Faults by Iterative Proportional-Integral Observers. *IEEE Trans. Fuzzy Syst.* **2022**, *30*, 542–554. [[CrossRef](#)]
22. Gu, Y.; Park, J.H.; Shen, M.; Liu, D. Event-triggered control of Markov jump systems against general transition probabilities and multiple disturbances via adaptive-disturbance-observer approach. *Inf. Sci.* **2022**, *608*, 1113–1130. [[CrossRef](#)]
23. Kong, S.; Sun, J.; Qiu, C.; Wu, Z.; Yu, J. Extended State Observer-Based Controller With Model Predictive Governor for 3-D Trajectory Tracking of Underactuated Underwater Vehicles. *IEEE Trans. Ind. Inform.* **2021**, *17*, 6114–6124. [[CrossRef](#)]
24. Zhang, Z.; Jing, L.; Wu, X.; Xu, W.; Liu, J.; Lyu, G.; Fan, Z. A Deadbeat PI Controller with Modified Feedforward for PMSM under Low Carrier Ratio. *IEEE Access* **2021**, *9*, 63463–63474. [[CrossRef](#)]
25. Lin, F.; Shen, P.; Kung, Y. Adaptive wavelet neural network control for linear synchronous motor servo drive. *IEEE Trans. Magn.* **2005**, *41*, 4401–4412.
26. Ortombina, L.; Tinazzi, F.; Zigliotto, M. Adaptive Maximum Torque per Ampere Control of Synchronous Reluctance Motors by Radial Basis Function Networks. *IEEE J. Emerg. Sel. Top. Power Electron.* **2019**, *7*, 2531–2539. [[CrossRef](#)]
27. Hou, Z.; Jin, S. *Model Free Adaptive Control*; Science Press: Beijing, China, 2013; pp. 124–130.
28. Hou, Z.; Xiong, S. On Model-Free Adaptive Control and Its Stability Analysis. *IEEE Trans. Autom. Control* **2019**, *64*, 4555–4569. [[CrossRef](#)]
29. Jin, S.; Hou, Z.; Wang, W. Model-free Adaptive Control Used in Permanent Magnet Linear Motor. In Proceedings of the 26th Chinese Control Conference, Zhangjiajie, China, 26 July–31 July 2007; pp. 1638–1641.
30. Cao, R.; Hou, Z. Model-free Learning Adaptive Control of Permanent Magnet Linear Motor. *Electr. Drive* **2006**, *7*, 22–25.
31. Cao, R.; Zheng, X.; Hou, Z. An Iterative Learning Control Based on Improved Multiple Input and Multiple Output Model Free Adaptive Control for Two-Dimensional Linear Motor. *Trans. China Electrotech. Soc.* **2021**, *36*, 4025–4034.
32. Cui, J.; Yan, H.; Shan, B. Direct Thrust Control of Permanent Magnet Linear Synchronous Motor Based on Model-free Adaptive Control Method. *Modul. Mach. Tool Autom. Manuf. Tech.* **2013**, *6*, 47–49+53.
33. Wang, Y.; Hou, Z. Model-free adaptive predictive control for PMSM systems with external disturbance. *Control. Theory Appl.* **2022**, *39*, 837–846.

-
34. Hashjin, S.A.; Pang, S.; Miliiani, E.; Ait-Abderrahim, K.; Nahid-Mobarakeh, B. Data-Driven Model-Free Adaptive Current Control of a Wound Rotor Synchronous Machine Drive System. *IEEE Trans. Transp. Electrification* **2020**, *6*, 1146–1156. [\[CrossRef\]](#)
 35. Mircea-Bogdan, R.; Raul-Cristian, R.; Radu-Emil, P. Multi-input–multi-output system experimental validation of model-free control and virtual reference feedback tuning techniques. *IET Control Theory Appl.* **2016**, *10*, 1395–1403.
 36. Han, J. *Active Disturbance Rejection Control Technology*; National Defense Industry Press: Beijing, China, 2008; pp. 197–207.
 37. Shao, L.; Liao, X.; Xia, Y.; Han, J. Stability Analysis and Synthesis of third order discrete extended state observer. *Inf. Control* **2008**, *37*, 135–139.